RSC Advances

PAPER

View Article Online
View Journal | View Issue

Cite this: *RSC Adv.*, 2020, **10**, 30077

Chitin derived biochar for efficient capacitive deionization performance

Pengwei Li,[a] Tao Feng,*[ab] Zhengyuan Song,[a] Yi Tan[a] and Weiwei Luo[a]

Received 25th June 2020
Accepted 31st July 2020

DOI: 10.1039/d0ra05554a

rsc.li/rsc-advances

The selection and preparation of an electrode material is the core of capacitive deionization. In order to obtain a material with a good deionization properties, we have designed an environmentally-friendly and simple way of preparing biochar. In this work, biochar was prepared by a thermal-deposition method and after chemical modification it was characterized with a scanning electron microscope (SEM), Fourier transform infrared spectrophotometer (FTIR), X-ray diffraction (XRD) and X-ray photoelectron spectroscopy (XPS). The specific surface area of biochar modified by KOH is as high as 833.76 m^2 g^{-1}, but the specific surface area of the unmodified electrode material is only 126.43 m^2 g^{-1}. The electrochemical analysis (CV and EIS) of the biochar indicates that HC-800 has a lower charge transfer resistance and a higher specific capacitance, where the specific capacity of HC-800 reaches 120 F g^{-1}. A CDI property analysis of HC-800 shows a better electrosorption capacity of 11.52 mg g^{-1} and better regeneration and cycling stability than CS-800. The desalination amount remains 87.23% after several cycles.

1. Introduction

Since the beginning of the 21st century, the three major issues of population, resources and the environment have become the challenges all humans must face. Among these, water resources, as an irreplaceable essential resource for mankind, have become one of the most urgent problems in the world.[1,2] Capacitive deionization technology is a new type of water treatment technology in which ions are moved to the oppositely charged electrode and adsorbed onto the electrical double-layer (EDL) formed between the solution and the electrode interface. Once the voltage is removed, the ions adsorbed by the electrodes can be immediately released into the solution.[3] CDI is regarded as a novel and promising alternative technology due to its low energy consumption, low cost, rapid regeneration and environmental friendliness and it is used for the removal of charged species from sea water and brackish water.[4–6] Therefore, capacitive deionization technology is considered to be a non-membrane desalination technology which is expected to replace the traditional desalination method.[7,8]

As the core component of the CDI module, the material electrode directly affects the desalination effect of CDI.[9] Biochar materials have been most widely applied in CDI electrodes, due to their wide range of sources, sustainable regeneration, excellent capacitance and low pollution.[10–12] Biomasses such as chitosan,[13] sugarcane,[14] *Artocarpus* peels,[15] bitter-tea and palm shell wastes,[16] and straw[3] have been widely used as precursors for preparing biochar materials. Chitin, which is second only to cellulose in yield, is an excellent raw material for biochar. Carbon prepared from chitin has a high surface area, well-developed mesoporosity and a high nitrogen content.[17] Most studies have shown that carbon materials with a high nitrogen content can improve the wettability of products, enlarging the accessible electrode area and enhancing charge accumulation, which is helpful for transferring charge during the electrosorption process and improves the specific capacitance.[13,18,19]

In recent years, the modification of biochar has been a research hotspot in improving the electroadsorption capacity of biochar electrodes. The main methods include acidification, physical modification by high-temperature carbonization in an atmosphere furnace and chemical modification by adding chemical activators such as KOH,[20–22] $ZnCl_2$,[23,24] *etc.*[25] KOH is commonly used in the preparation of biochar with a high specific surface area, which not only has excellent water absorption, but can also greatly improve the specific surface area and pore structure of biochar by reacting with carbon atoms to produce gases or salt solids in the thermal decomposition process, and which plays the role of pore making and space occupation.[26] Meanwhile, the specific surface area and pore structure of the biochar electrode are important parameters affecting the electrode's electrosorption property.[27,28] Previous studies have shown that chitin is a suitable precursor for porous carbon materials that have been applied in supercapacitors[29,30] and lithium ion batteries.[31,32] However, the electrosorption behavior of chitin derived biochar during CDI is still

[a]*College of Resources and Environmental Engineering, Wuhan University of Science and Technology, Wuhan 430081, China. E-mail: fengtaowhu@163.com*

[b]*Hubei Key Laboratory for Efficient Utilization and Agglomeration of Metallurgic Mineral Resources, Wuhan University of Science and Technology, Wuhan 430081, China*

unknown. Meanwhile, in order to improve the electroadsorption capacity of chitin derived biochar, the influence of the activator KOH on the structure, surface morphology, specific surface area, pore size structure, electrochemical property and CDI property of chitin derived biochar are worth studying.

In this work, the biochar was prepared by carbonizing chitin under nitrogen protection in a tube furnace followed by KOH-activation. The influence of KOH on the structure, morphology, electrochemical property and CDI property was studied by comparing KOH-activated biochar with biochar. The two kinds of biochar were characterized by BET, SEM, XRD, FTIR and XPS. The electrochemical properties of the two kinds of biochar electrodes were tested by cyclic voltammetry and electrochemical impedance spectroscopy (EIS) at an electrochemical workstation. The capacitive deionization, regeneration and cycling stability of the two kinds of biochar electrodes were tested with a simple home-made electroadsorption device. KOH-activated chitin derived biochar electrode is a new option for a CDI electrode.

2. Experimental

2.1 Materials

Chitin; polyvinylidene fluoride (PVDF), KOH, NaOH, HCl and *N*,*N*-dimethylacetamide (DMAC) were purchased form Sinopharm Chemical Reagent Co., Ltd. Conductive carbon black was obtained from Tianjin Jindadi Chemical Co., Ltd. All chemicals are analytical reagents.

2.2 Synthesis of biochar

An appropriate amount of chitin was heated up to 400 °C at 5 °C min^{-1} in a tubular furnace (SK-GO5123K, Tianjin Zhonghuan Electric Furnace, China) and cooled to obtain pre-carbonized chitin. The pre-carbonized chitin fully blended with the activator KOH (0 g and 25% mass of pre-carbonized chitin) was heated up to the target temperature (800 °C) and kept for 2 hours under a nitrogen atmosphere, where the nitrogen flow rate was 100 mL min^{-1}. After naturally cooling to ambient temperature, the product was cleaned thoroughly with 10% HCl to completely remove the remaining residues, and rinsed with distilled water several times to pH = 7. Finally the product was dried for 10 h in an oven at 80 °C. The two obtained biochars were named CS-800 and HC-800, according to whether KOH was used.

2.3 Characterization

The morphological characteristics of CS-800 and HC-800 were observed by scanning electron microscopy (S4800, Hitachi, Japan). The specific surface area and pore size distribution analysis of CS-800 and HC-800 were investigated with an automatic surface area and porosity analyser (ASAP2020, Micromeritics, USA). The CS-800 and HC-800 were ground into powder, then formed into tablets with KBr (sample mass 1%). FTIR spectrometry of CS-800 and HC-800 were recorded on a Nicolet-460 FTIR spectrometer (Madison, Nicolet, USA) over the wave range of 4000 to 400 cm^{-1}. The crystal structures of CS-800 and HC-800 were investigated with an X-ray diffractometer (APEXII, Bruker, USA). The chemical compositions of CS-800 and HC-800 were analyzed using X-ray photoelectron spectroscopy (XPS; Escalab 250 XI, Thermo Fisher, USA).

2.4 Electrode sheet fabrication and electrochemical analysis

CS-800 and HC-800 were mixed with conductive carbon black and polyvinylidene fluoride at a weight ratio of 75 : 5 : 20 with dimethylacetamide as the solvent. The mixture was stirred in a magnetic stirrer for 1 h after ultrasonication for 10 min. The obtained mixture was uniformly coated on both sides of a titanium sheet to prepare a 6 × 5 cm electrode sheet followed by drying in a vacuum oven at 50 °C for 4 hours. The effective mass of an electrode is about 0.35 g.

The electrochemical properties of the HC-800 and CS-800 electrodes were tested by CV and EIS tests at an electrochemical workstation (CHI660E, Shanghai Chenhua Instrument Co. Ltd). The concentrations of electrolyte in the CV test and EIS test were 0.5 mol L^{-1} and 0.05 mol L^{-1} KCl, respectively. A three-electrode working system was adopted in the testing system. An Ag/AgCl electrode, the prepared biochar electrodes and a platinum wire electrode were the reference electrode, working electrode and counter electrode, respectively. The whole testing process was carried out at room temperature. The frequency of the EIS test ranged from 0.01 Hz to 10 000 Hz, and the amplitude was 5 mV. The capacitance (C, F g^{-1}) of the HC-800 and CS-800 electrodes can calculated from eqn (1) according to the current–voltage curves obtained from the CV test:[33,34]

$$C_S = \int_{U_i}^{U_f} I \frac{1}{vm(U_f - U_i)} dU \quad (1)$$

where I (A) is the current; U_f (V) and U_i (V) are the final voltage and initial voltage, respectively, the scanning voltage ranges from −1.2 V to 1.2 V; v (V s^{-1}) is the scanning rate, where the scanning rates were 0.02 V s^{-1}, 0.01 V s^{-1}, 0.005 V s^{-1} and 0.002 V s^{-1}, respectively. The effective mass (m) of an electrode is about 0.35 g.

2.5 CDI experiment

The capacitive deionization properties, regeneration and cycling stability of the HC-800 and CS-800 electrodes were tested by a simple home-made electroadsorption device, which consisted of a CDI module, a DC power supply (IT6322, ITECH, China), a peristaltic pump, a beaker and a conductivity meter (DDB-12L, TUNE VOLT, China). A constant direct voltage of 2 V was applied to two electrode plates of the same biochar whose distance was 8 mm. 300 mL of NaCl solution (50 μs cm^{-1}, 160 μs cm^{-1}, 300 μs cm^{-1}, 500 μs cm^{-1}) was circulated between the CDI module and the beaker at a flow rate of 20 mL min^{-1} by a peristaltic pump. The change in concentration (y) which has a good linear relationship with conductivity (x), was monitored and recorded with a conductivity meter throughout the experiments ($y = 2.4119x + 38.346$).

Electrosorption capacity (q) and rate of desalination (η) were calculated from eqn (2) and (3), respectively:

$$q = \frac{(c_0 - c)}{mM} \times V \quad (2)$$

$$\eta = \frac{c_0 - c}{c_0} \times 100\% \quad (3)$$

where c_0 and c are the initial and equilibrium concentrations (mg L^{-1}) of NaCl, V (L) represents the volume of the NaCl solution (0.3 L), m (g) represents the effective mass of two electrodes (0.7 g), and M represents the relative molecular weight of NaCl (58.5 g mol^{-1}).

3. Results and discussion

3.1 Structure and morphological characterization

Scanning electron microscopy (SEM) was used to observe the pore morphology and surface morphology of chitin powder and biochar powder. As shown in Fig. 1a and b, the chitin powders are irregular particles with a size of several hundred micrometers, and the particles are tight, blocky and compact. The original powder particles are not uniform, and have no substantial intermolecular pores. After high-temperature carbonization, the scanning electron microscopy images (such as Fig. 1c and d) of CS-800 show that the size of the particles shrinks significantly, which is consistent with the macroscopic observation of the two samples. It can be seen from the high-magnification image that the surface of the CS-800 particles becomes fluffy and porous, which may be caused by the escape of various small molecules from the chitin powder during high-temperature carbonization. Fig. 1e and f are scanning electron microscope images of HC-800, which were obtained by comparison with the scanning electron microscope image of Fig. 1c and d for CS-800. After modification, new holes are formed due to the reaction of KOH with chitin. The size of the biomass carbon powders shrinks further, and the structure of pores and voids is more complicated, making it possible that HC-800 has a larger specific surface area. Since the lamellar structure of HC-800 greatly increases the porosity of chitin and the sheet-like particle size is thin, the generated pores can be effectively utilized in the subsequent utilization.

The specific surface area and pore diameter distribution of the electrode are important factors affecting the adsorption properties of the electrode. Fig. 2 illustrates the N_2 adsorption/desorption isotherms of CS-800 and HC-800 at −196 °C. The adsorption isotherm of CS-800 is similar to a type IV isotherm which indicates that the CS-800 contains a certain amount of mesopores.[35,36] According to the IUPAC classification, the hysteresis loop of the CS-800 adsorption curve belongs to type H3 which indicates that the particles of CS-800 are flaky. From the adsorption isotherm of the modified biochar HC-800, it can be seen that the adsorption amount in the low-pressure zone increases rapidly, and the adsorption amount in the medium pressure zone changes little. The adsorption curve of HC-800 belongs to type I, and thus it can be judged that the modified biochar HC-800 contains mainly micropores and contains a certain amount of mesopores.[37,38] Fig. 3 shows that the pore sizes of CS-800 mainly range from 2 nm to 10 nm, while the pore size of HC-800 ranges from 2 nm to 6 nm, which is consistent with previous N_2 adsorption/desorption isotherm analysis results.[39] Table 1 shows the microstructure parameters of CS-800 and HC-800. The specific surface area of HC-800 (833.76 m^2 g^{-1}) is 6.59 times that of CS-800 (123.43 m^2 g^{-1}). The micropore volume accounts for about 77.8% of the total pore volume, which indicates that most pores of HC-800 are micropores. The increased specific surface area and micropores are very beneficial for the formation of double-layer capacitors in the process of capacitor deionization and in enhancing the CDI property.

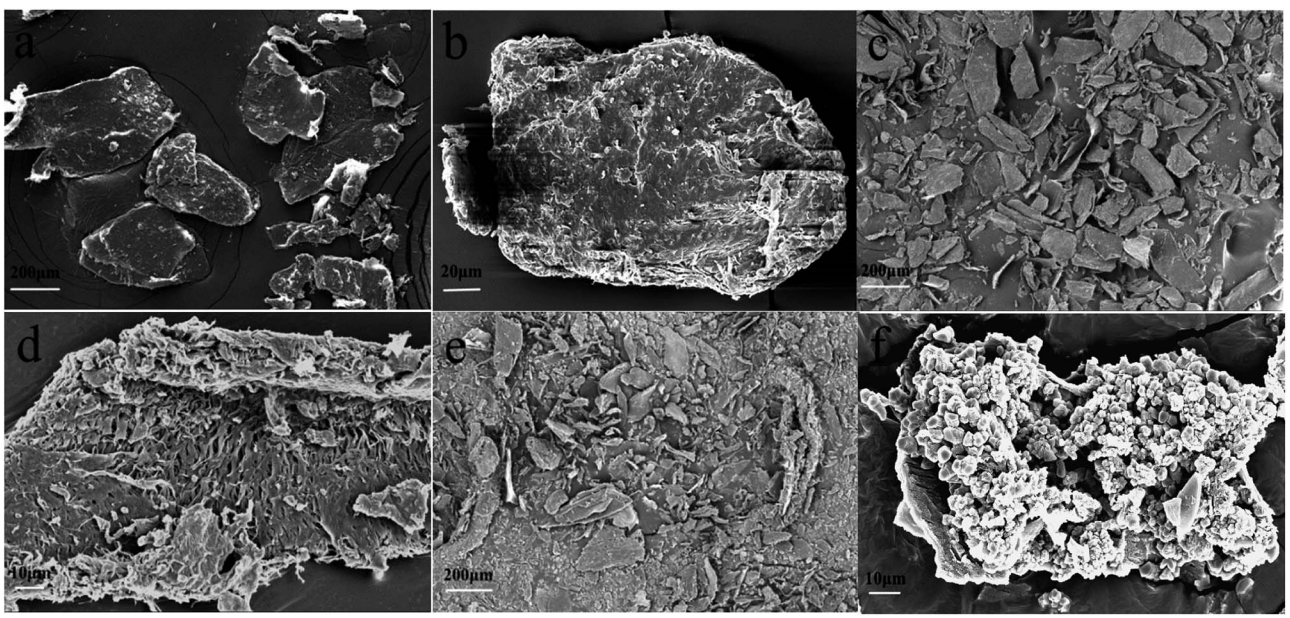

Fig. 1 SEM images of chitin (a and b), CS-800 (c and d) and HC-800 (e and f).

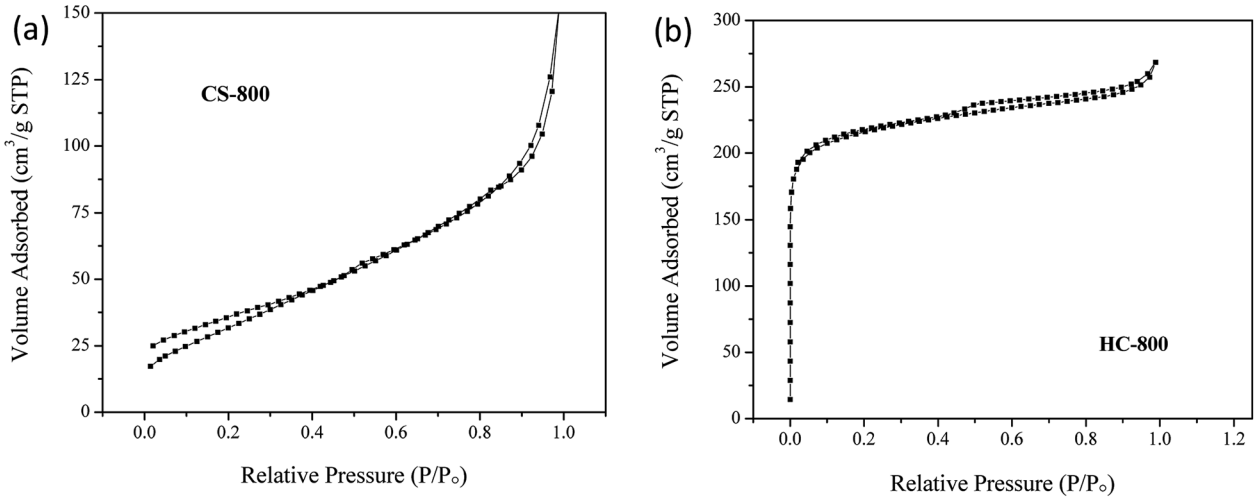

Fig. 2 N_2 adsorption/desorption isotherms of CS-800 (a) and HC-800 (b) at −196 °C.

Fig. 4a shows the FTIR spectra of HC-800 and CS-800. It can be seen that the absorption peaks at 3433 cm^{-1}, 1628 cm^{-1} and 1108 cm^{-1} underwent no shift. The peak at 3433 cm^{-1} is attributed to the O–H stretching vibration, indicating that both kinds of biochar contain a certain amount of hydroxyl, and the asymmetry of the CS-800 middle peak is attributed to the existence of hydrogen bonding. But the addition of KOH destroys the hydrogen bonding. The peak at 1630 cm^{-1} is due to the stretching vibration of C=O. The peak at 1108 cm^{-1} is assigned to the stretching vibration of C–O in the secondary alcohol. A new characteristic peak of HC-800 at 620 cm^{-1} was formed by the in-plane bending vibration of C–CO–C.

Fig. 4b shows the XRD patterns of CS-800 and HC-800. The characteristic peaks of CS-800 appeared at $2\theta = 24.85°$ and 29.44°. These sharp diffraction peaks indicated that there was a certain crystalline region in CS-800. But the diffraction peaks in HC-800 were weaker and wider than those in CS-800, where no new peaks arose after modification. The cause of this change was that the KOH and CS-800 did not produce a chemical reaction to form a new substance, but the addition of KOH affected the degree of crystallization of CS-800. The degree of crystallization of the biochar was reduced, so the structure of HC-800 is looser than that of CS-800. The XPS peaks of C, N and O in CS-800 and HC-800 are shown in Fig. 5. Fig. 5a shows that there are four main forms of carbon in CS-800 and HC-800, which are C–C, C–O, C=O, and –COOH. Fig. 5b shows that nitrogen exists in CS-800 and HC-800 in three main forms, which are pyrrolic-N (N-5), pyridinic-N (N-6) and graphitic-N (N-Q). Table 2 indicates that HC-800 has a higher content of pyrrolic-N (N-5) and graphitic-N (N-Q). As HC-800 has more abundant pore channels than CS-800, it is easier to lose nitrogen atoms from the surface, so the nitrogen content of HC-800 surface is slightly lower than that of CS-800. Fig. 5c shows that the main forms of oxygen in CS-800 and HC-800 are C=O (O-I), –O– (O-II) and –COOH (O-III). Oxygen finds it difficult to escape during thermal decomposition and KOH activation, so the oxygen content of CS-800 and HC-800 is very high, but the existing forms of oxygen are significantly different: the O-III of CS-800 is much greater than the O-III of HC-800, suggesting that activator KOH not only changes the morphological structure of biochar, but also to some extent changes the composition.

By analyzing and comparing the structure and composition of CS-800 and HC-800, the reaction process of hole formation and KOH activation can be inferred. When the chitin powder is carbonized to form CS-800, the chitin itself is compact and the intermolecular forces are relatively large. The intermediates formed in the carbonization process are relatively compact, and the small molecular gases formed in the thermal decomposition process find it difficult to escape, resulting in the inconspicuous pore-making effect. After adding the activator KOH,

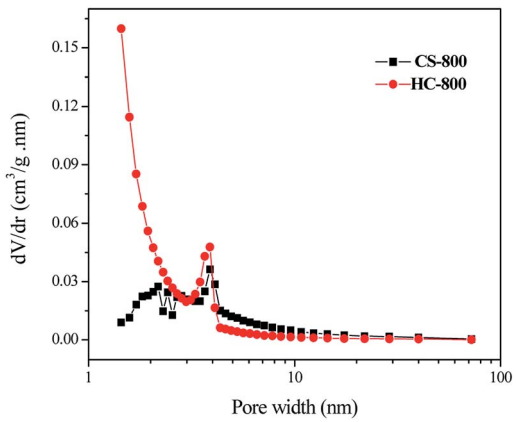

Fig. 3 Pore size distribution (BJH) of CS-800 and HC-800.

Table 1 Microstructure parameters of CS-800 and HC-800

Samples	S_{BET} m^2 g^{-1}	S_{BJH} m^2 g^{-1}	V_{BJH} cm^3 g^{-1}	R_{BJH} nm
CS-800	126.43	41.54	0.13	6.91
HC-800	833.76	118.55	0.24	4.36

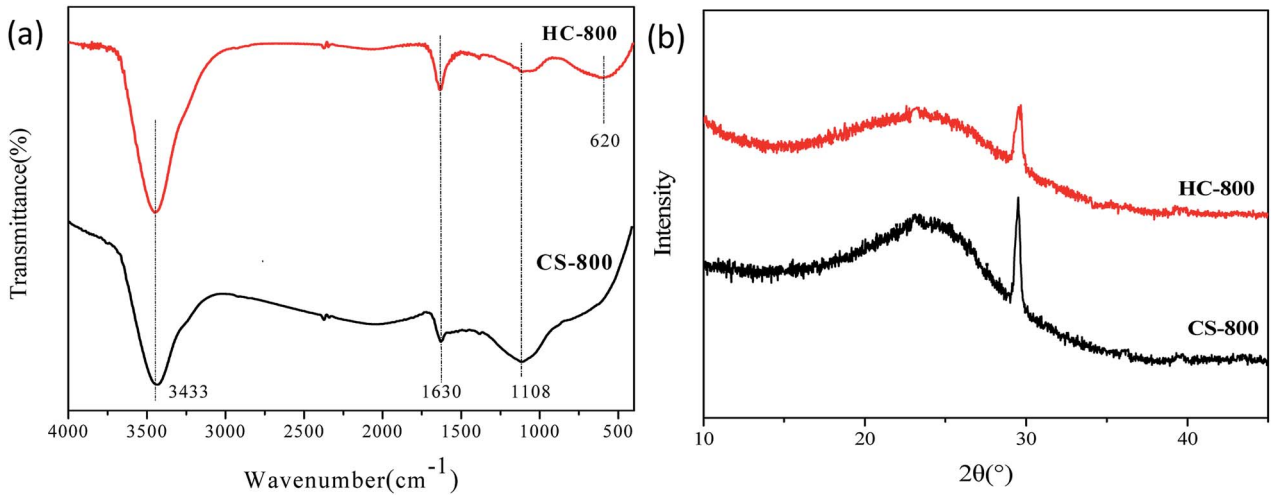

Fig. 4 (a) The FTIR spectra of HC-800 and CS-800, (b) X-ray diffraction analysis of various CS-800 and HC-800.

some chemical reactions will occur, as shown in eqn (4)–(6), where $-CH_2OH$ is used to represent the part of the groups participating in the reaction. In the high temperature process, KOH not only reacts with some groups in chitin, but also with the gases (CO and H_2) generated by the reaction of KOH with carbon atoms and the metallic potassium salt, which can play the role of making pores and occupying space, greatly improving the specific surface area of HC-800 and enriching the pore structure. The adhesion of sylvite to the biochar material in the molten state can also reduce its surface tension and reduce

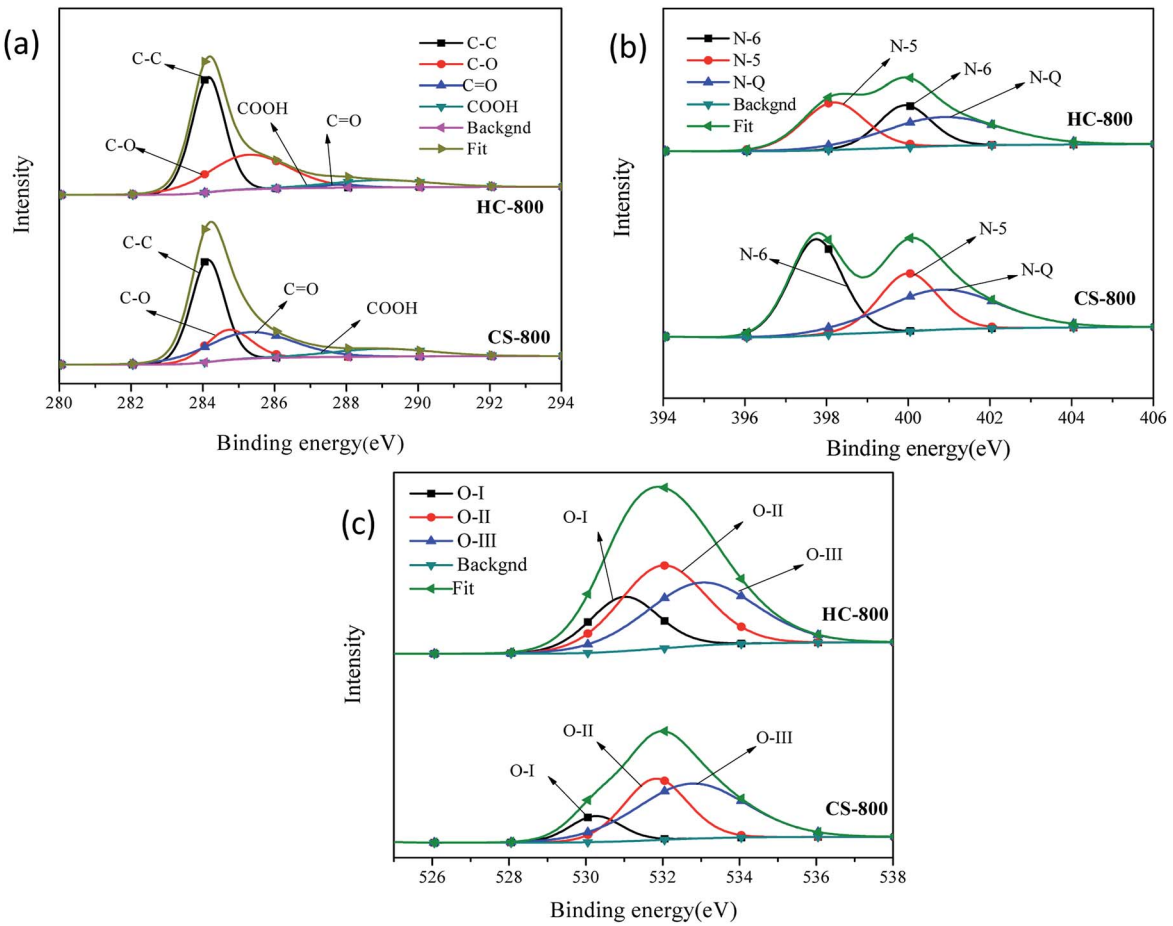

Fig. 5 XPS spectra of HC-800 and CS-800, (a) C spectrum, (b) N spectrum, (c) O spectrum.

Table 2 The different forms of O and N contents of HC-800 and CS-800 from the element analyzer

	N [%]			O [%]		
Samples	N-5 [%]	N-6 [%]	N-Q [%]	O-I [%]	O-II [%]	O-III [%]
CS-800	6.22			14.53		
	25.71	38.75	35.54	11.91	34.46	53.63
HC-800	4.85			13.78		
	25.94	34.57	39.49	21.02	40.15	38.83

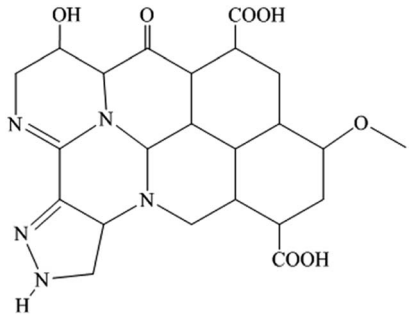

Fig. 6 Structure diagram of O and N on ideal HC-800.

the mass transfer resistance of the electrolyte in the carbon material, thus boosting the electrochemical property of HC-800.

$$4KOH + (-CH_2OH) \rightarrow K_2CO_3 + K_2O + 3H_2\uparrow + (-H) \quad (4)$$

$$K_2CO_3 + 2C \rightarrow 2K + 3CO\uparrow \quad (5)$$

$$K_2O + C \rightarrow 2K + CO\uparrow \quad (6)$$

As shown in Fig. 6, the possible structure of HC-800 can be roughly guessed at. According to previous characterizations, it can be seen from SEM that the carbon material has an extremely thin flaky particle structure. Different characteristic peaks of FTIR analysis can determine the functional groups of HC-800. XPS analysis further provides the types and contents of the functional groups.

3.2 Electrochemical analysis of HC-800 electrode and CS-800 electrode

Fig. 7 shows the CV curves of CS-800 and HC-800 at different scan rates. More precisely, the specific capacitances of CS-800 at 0.02 V s^{-1}, 0.01 V s^{-1}, 0.005 V s^{-1} and 0.002 V s^{-1} were estimated as 24.85 F g^{-1}, 29.17 F g^{-1}, 34.66 F g^{-1} and 42.87 F g^{-1}, respectively. The specific capacitances of HC-800 at 0.02 V s^{-1}, 0.01 V s^{-1}, 0.005 V s^{-1} and 0.002 V s^{-1} were estimated as 50.91 F g^{-1}, 64.86 F g^{-1}, 82.12 F g^{-1} and 122.33 F g^{-1}, respectively. If the energy storage mechanism was through non-faradaic EDL phenomena, the CV curve would exhibit a rectangle.[40–42] However, the CV curves of CS-800 and HC-800 are not ideal rectangles, which may be caused by other redox reactions occurring in the electrolysis system, resulting in the irregular shape of the scanning pattern. By comparing the adsorption capacity of different scanning rates, the capacitance of the electrode decreases with the increase in the scanning rate, which may be because the scanning rate is so fast that ions are too slow to enter into the pores of the biochar.[43] The CV curves of the CS-800 electrodes were compared with the CV curves of the HC-800 electrodes, and it was found that the HC-800 electrodes have a better electrochemical property.

The chemical impedance test can reflect the dynamics of the charge transfer and substance diffusion at the electrode/solution interface. Fig. 8a shows the EIS spectra of the HC-800 electrode and CS-800 electrode, and the diameter of the arc

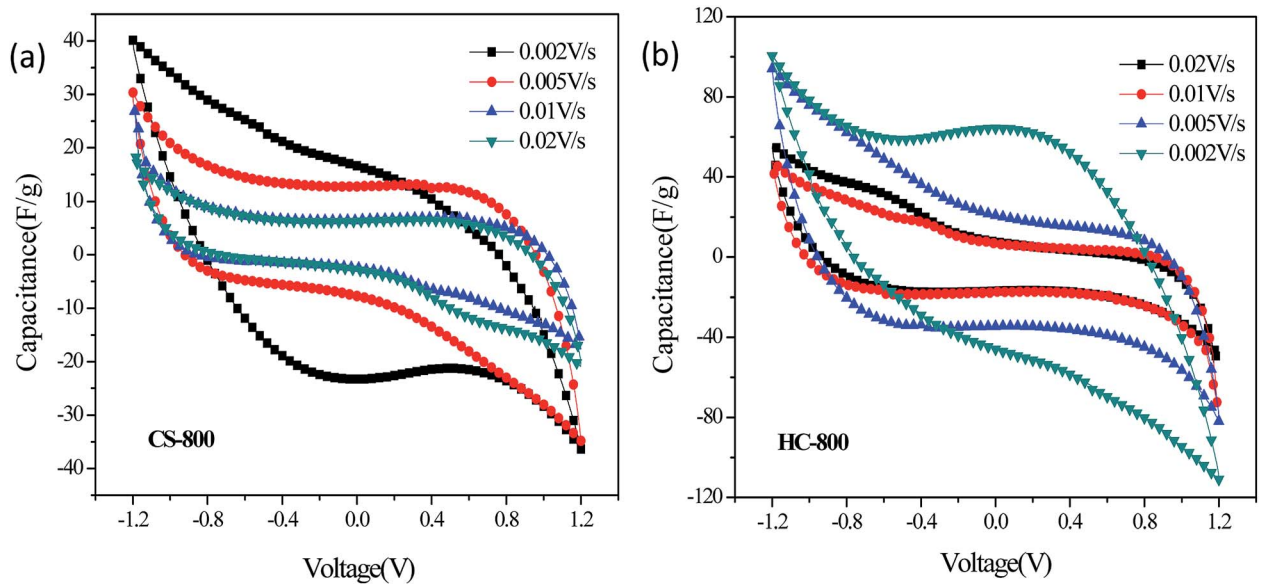

Fig. 7 CV curves of CS-800 (a) and HC-800 (b) at different scan rates.

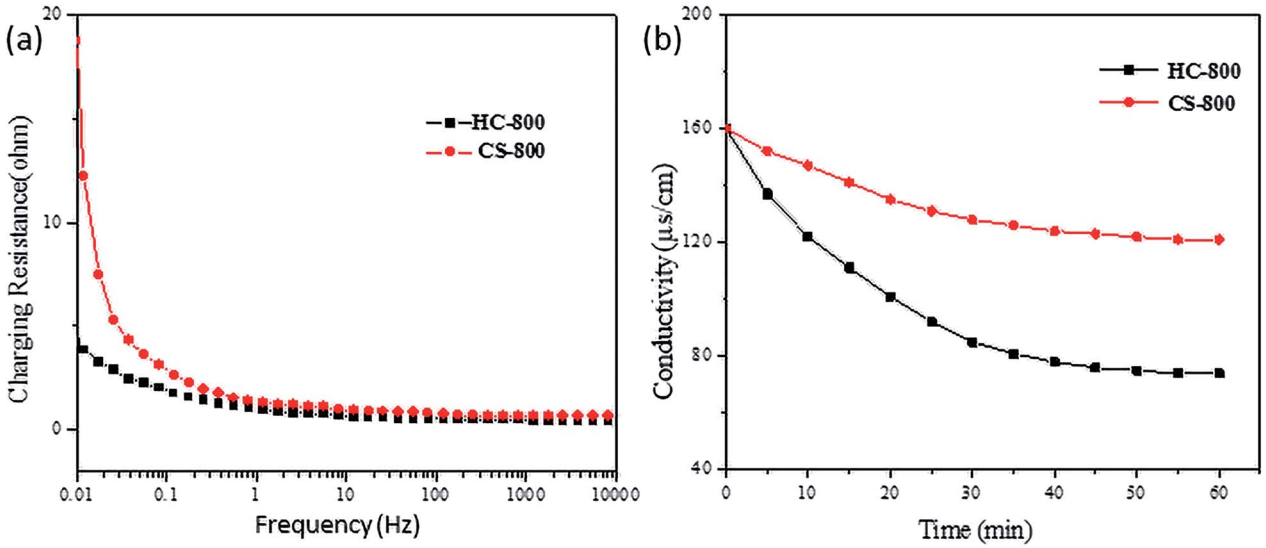

Fig. 8 (a) EIS curves of HC-800 and CS-800. (b) Solution conductivity *vs.* time for HC-800 electrode and CS-800 electrode in the process of capacitive deionization and desalination.

can reflect the diffusion resistance of ions at the interface between NaCl solution and biochar electrode. The diameter of the arc is proportional to the ionic diffusion resistance.[44] In the low-frequency region, the slope of the HC-800 electrode is larger than that of the CS-800 electrode, indicating that after KOH activation, the HC-800 electrode has a larger capacitance and a smaller ionic diffusion resistance. In the high-frequency region, the arc diameter of the CS-800 electrode is larger than that of the HC-800 electrode, which could imply that ionic mass transfer resistance between CS-800 electrode and solution was greater than that from the HC-800 electrode. After KOH activation, the electrochemical properties of HC-800 were significantly improved in all aspects at all frequencies, such as the ionic mass transfer resistance of the biochar electrodes and solution being reduced and the capacitance of the biochar electrode being increased, which significantly improved the adsorption effect in the process of CDI.

3.3 CDI experiment of HC-800 electrode and CS-800 electrode

The most straightforward method to compare the CDI properties of HC-800 and CS-800 is to conduct capacitive deionizing and desalting experiments. Fig. 8b shows the change in conductivity in the process of capacitive deionization and desalination. During the deionization process of the CS-800 electrode, the conductivity of the solution decreased from 160 μs cm^{-1} to 121 μs cm^{-1}, and the salt removal efficiency of CS-800 was 24.37%. For the HC-800 electrode, the solution conductivity decreased from 160 μs cm^{-1} to 74 μs cm^{-1}, and the

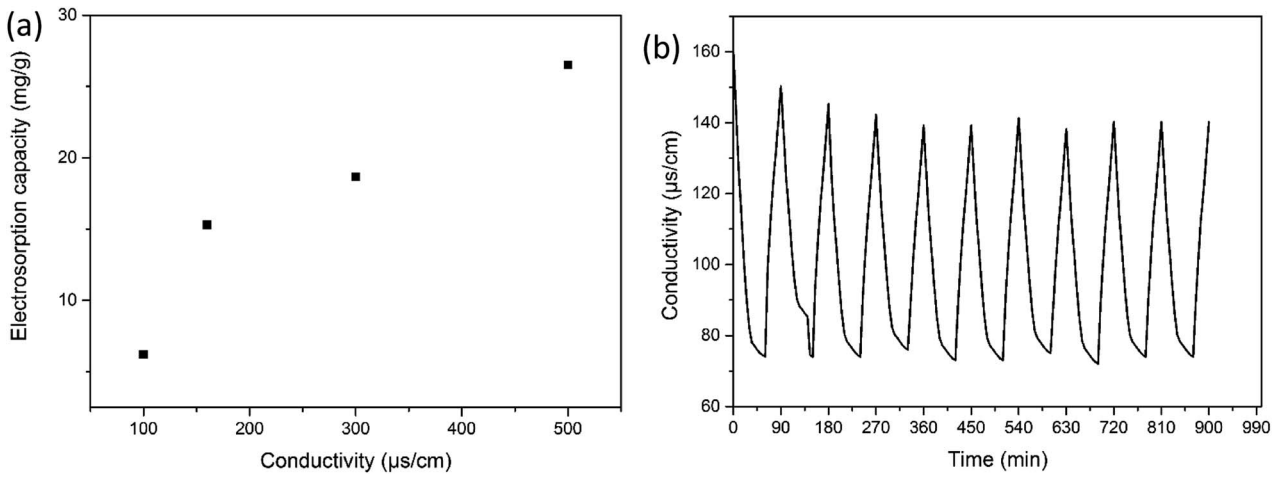

Fig. 9 (a) Electrosorption capacity of HC-800 electrodes at different concentration of NaCl solution. (b) Cycling stability performance of HC-800.

salt removal efficiency of the HC-800 electrode was 53.75%. The electroadsorption capacities of the HC-800 electrode and the CS-800 electrode were 15.4 mg g^{-1} and 6.93 mg g^{-1}, respectively. The HC-800 electrode showed a better electrosorption property than CS-800.

It can be seen from Fig. 9a that the higher the concentration of the solution, the higher the electrosorption capacity. This is mainly due to the fact that the micropores inside the materials can improve the ion mass transfer rate and reduce the overlap effect in higher concentration solutions.[45] When the conductivity of the solution increases from 50 to 500 μs cm^{-1}, the electrosorption capacity increases from 6.2 to 26.5 mg g^{-1}. The electrosorption capacity of the HC-800 electrodes with 500 μs cm^{-1} of NaCl solution is also higher than for most biochar materials reported in the literature, such as chitosan-based activated carbon,[13] soybean shells,[46] pine pollen,[39] or sugarcane biowaste derived biochars.[14]

Regeneration and cycling stability are also important parameters in choosing good CDI electrode materials. Fig. 9b shows the adsorption and desorption process of the modified biomass carbon electrode. When the positive and negative plates are short-circuited, the conductivity of the solution continues to increase, indicating that the electrode has begun to desorb, and the desorption time is half as fast as the electrosorption time. After using for a period of time, the electrosorption property of the electrode is the same as it was initially, the surface is intact, and no peeling has occurred. It could be observed that the HC-800 electrode exhibited a maximum charge efficiency of 87.23% after several cycles, indicating that the HC-800 electrode has excellent regeneration and cycling stability.

4. Conclusions

Porous biochar derived from chitin has been successfully synthesized by a thermal-deposition method followed by KOH-activation. The KOH-activated biochar (HC-800) with abundant micropores and a high specific surface area exhibits the best electrochemical and desalination performance compared with biochar without any additives (CS-800). The specific surface area of HC-800 is as high as 833.76 m^2 g^{-1}, compared with the 126.43 m^2 g^{-1} of CS-800. The maximum capacity of HC-800 is 122.33 F g^{-1}, compared with the 42.87 F g^{-1} of CS-800. The charging resistance of HC-800 is 4.16 Ω, compared with the 18.75 Ω of CS-800. The HC-800 electrode showed better electrosorption capacity than CS-800. HC-800 exhibited a maximum charge efficiency of 87.23% after several cycles, and HC-800 has good cyclic desalination stability and regeneration ability. Therefore, HC-800 provides a promising and environmentally-friendly method for a capacitive deionization device.

Conflicts of interest

There are no conflicts to declare.

Acknowledgements

This work was supported by Technology Innovation Special Foundation of Hubei Province (2019ACA152 and 2019ZYYD060).

References

1 Z. Xie, X. Shang, J. Yan, T. Hussain, P. Nie and J. Liu, Biomass-derived porous carbon anode for high performance capacitive deionization, *Electrochim. Acta*, 2018, **290**, 666.
2 M. Elimelech and W. A. Phillip, The future of seawater desalination: energy, technology, and the environment, *Science*, 2011, **333**, 712.
3 H. Wang, T. T. Yan, J. J. Shen, J. P. Zhang, L. Y. Shi and D. S. Zhang, Efficient removal of metal ions by capacitive deionization with straw waste derived graphitic porous carbon nanosheets, *Environ. Sci.: Nano*, 2020, **7**, 317.
4 G. Z. Wang, T. T. Yan, J. P. Zhang, L. Y. Shi and D. S. Zhang, Trace-Fe-Enhanced Capacitive Deionization of Saline Water by Boosting Electron Transfer of Electro-Adsorption Sites, Environmental Science & Technology, *Environ. Sci. Technol.*, 2020, **54**, 8411–8419.
5 Z. U. Khan, T. T. Yan, J. Han, L. Y. Shi and D. S. Zhang, Capacitive deionization of saline water using graphene nanosphere decorated N-doped layered mesoporous carbon frameworks, *Environ. Sci.: Nano*, 2019, **6**, 3442.
6 D. Li, L. Shen and S. Jiang, Development and application of electrosorption technology, *J. Water Resour. Prot.*, 2008, **24**, 63.
7 C. Zhang, D. He and J. Ma, Faradaic reactions in capacitive deionization (CDI) problems and possibilities: a review, *Water Res.*, 2018, **128**, 314.
8 T. J. Welgemoed and C. F. Schutte, Capacitive Deionization Technology: an alternative desalination solution, *Desalination*, 2005, **183**, 327.
9 J. L. Han, T. T. Yan, J. J. Shen, L. Y. Shi, J. P. Zhang and D. S. Zhang, Capacitive Deionization of Saline Water by Using MoS_2^- Graphene Hybrid Electrodes with High Volumetric Adsorption Capacity, *Environ. Sci. Technol.*, 2019, **53**, 12668–12676.
10 M. Noked, A. Soffer and D. Aurbach, The electrochemistry of activated carbonaceous materials: past, present, and future, *J. Solid State Electrochem.*, 2011, **15**, 1563.
11 C. Ruan, K. Ai and L. Lu, Biomass-derived carbon materials for high-performance supercapacitor electrodes, *RSC Adv.*, 2014, **4**, 30887.
12 Y. Liu, C. Y. Nie, X. J. Liu, X. T. Xu, Z. Sun and L. K. Pan, Review on carbon-based composite materials for capacitive deionization, *RSC Adv.*, 2015, **5**, 15205–15225.
13 Q. H. Wu, D. W. Liang, X. M. Ma, S. F. Lu and Y. Xiang, Chitosan-based activated carbon as economic and efficient sustainable material for capacitivedeionization of low salinity water, *RSC Adv.*, 2019, **9**, 26676.
14 J. L. Julio, L. Z. Rafael, I. V. Rodríguez, K. M. Barcelos and A. M. R. Luís, Sugarcane Biowaste-Derived Biochars as

Capacitive Deionization Electrodes for Brackish Water Desalination and Water-Softening Applications, *ACS Sustainable Chem. Eng.*, 2019, **7**, 18992–19004.

15 J. Isadiki, Y. A. C. Jande, R. L. Machunda and T. E. Kibona, Porous Carbon Derived from Artocarpus Heterophyllus Peels for Capacitive Deionization Electrodes, *Carbon*, 2019, **147**, 582–593.

16 P. A. Chen, H. C. Cheng and H. P. Wang, Activated Carbon Recycled from Bitter-Tea and Palm Shell Wastes for Capacitive Desalination of Salt Water, *J. Cleaner Prod.*, 2018, **174**, 927–932.

17 J. W. Robin, M. Antonietti and M.-M. Titirici, Naturally inspired nitrogen doped porous carbon, *J. Mater. Chem.*, 2009, **19**, 8645.

18 Y. Li, I. Hussain, J. W. Qi, C. Liu, J. S. Li, J. Y. Shen, X. Y. Sun, W. Q. Han and L. J. Wang, N-doped hierarchical porous carbon derived from hypercrosslinked diblock copolymer for capacitive deionization, *Sep. Purif. Technol.*, 2016, **165**, 190.

19 X. Xu, L. Pan, Y. Liu, T. Lu and Z. Sun, Enhanced capacitive deionization performance of graphene by nitrogen doping,*J. Colloid Interface Sci.*, 2015, **445**, 143.

20 R. J. Mo, Y. Zhao and M. Wu, Activated carbon from nitrogen rich watermelon rind for high-performance supercapacitor, *RSC Adv.*, 2016, **6**, 59333.

21 Y. Shu, A. Dobashi and C. Li, Hierarchical porous carbon from greening plant shell for electric double-layer capacitor application, *Bull. Chem. Soc. Jpn.*, 2016, **90**, 44.

22 A. M. Dehkhoda, E. Gyenge and N. Ellis, A novel method to tailor the porous structure of KOH-activated biochar and its application in capacitive deionization and energy storage, *Biomass Bioenergy*, 2016, **87**, 107.

23 T. E. Rufford, D. Hulicova-Jurcakova and Z. Zhu, Nanoporous carbon electrode from waste coffee beans for high performance supercapacitors, *Electrochem. Commun.*, 2008, **10**, 1594.

24 J. Zhang, L. Gong and J. Jiang, Preparation of activated carbon from wasteCamellia oleifera shell for supercapacitor application, *J. Solid State Electrochem.*, 2012, **16**, 2179.

25 P. Hao, Z. Zhao and Y. Leng, Graphene-based nitrogen self-doped hierarchical porous carbon aerogels derived from chitosan for high performance supercapacitors, *Nano Energy*, 2015, **15**, 9.

26 T. Guo, K. Dong and Y. Cai, Research progress and prospect of electrode materials for capacitive deionization technology, *Advanced materials frontier academic conference*, 2016, vol. 30, p. 7.

27 A. M. Dehkhoda, E. Gyenge and N. Ellis, Effect of activated biochar porous structure on the capacitive deionization of NaCl and $ZnCl_2$ solutions, *Microporous Mesoporous Mater.*, 2016, **224**, 217–228.

28 R. J. White, M. Antonietti and M. M. Titirjci, Naturally inspired nitrogen doped porous carbon, *J. Mater. Chem.*, 2009, **19**, 8645.

29 M. Z. Chu, Y. Y. Zhai, N. Z. Shang, P. J. GuO, C. Wang and Y. J. Gao, N-doped carbon derived from the monomer of chitin for high-performance supercapacitor, *Appl. Surf. Sci.*, 2020, **517**, 146140.

30 L. Yao, Nitrogen-doped Porous Carbon Derived from Chitin with Enhanced Performances for Oxygen Reduction Reaction and Supercapacitor, *Int. J. Electrochem. Sci.*, 2018, 5798.

31 R. Gurav, S. K. Bhatia, T.-R. Choi, H.-R. Jung, S.-Y. Yang, H.-S. Song, Y.-L. Park, Y.-H. Han, J.-Y. Park, Y.-G. Kim, K.-Y. Choi and Y.-H. Yang, Chitin biomass powered microbial fuel cell for electricity production using halophilic Bacillus circulans BBL03 isolated from sea salt harvesting area, *Bioelectrochemistry*, 2019, **130**, 107329.

32 C. Chen, Z. Wang, B. Zhang, L. Miao, J. Cai and L. Peng, Nitrogen-rich hard carbon as a highly durable anode for high-power potassium-ion batteries, *Energy Storage Mater.*, 2017, **8**, 161.

33 Y. Liu, T. Chen and T. Lu, Nitrogen-doped porous carbon spheres for highly efficient capacitive deionization, *Electrochim. Acta*, 2015, 403.

34 M. D. Stoller and R. S. Ruoff, Best practice methods for determining an electrode material's performance for ultracapacitors, *Energy Environ. Sci.*, 2010, **3**, 1294.

35 Y. Lu, S. Zhang and J. Yin, Mesoporous activated carbon materials with ultrahigh mesopore volumeand effective specific surface area for high performance supercapacitors, *Carbon*, 2017, **124**, 64.

36 H. Wang, L. Shi and T. Yan, Design of graphene-coated hollow mesoporous carbon spheres as high performance electrodes for capacitive deionization, *J. Mater. Chem. A*, 2014, **2**, 4739.

37 J. Wei, D. Zhou and Z. Sun, A controllable synthesis of rich nitrogen-doped ordered mesoporous carbon for CO2 capture and supercapacitors, *Adv. Funct. Mater.*, 2013, **23**, 2322.

38 Z. Li, Z. Xu and X. Tan, Mesoporous nitrogen-rich carbons derived from protein for ultra-high capacity battery anodes and supercapacitors, *Energy Environ. Sci.*, 2013, **6**, 871.

39 Q. Liu, X. Li and Y. Wu, Pine pollen derived porous carbon with efficient capacitive deionization performance, *Electrochim. Acta*, 2019, **298**, 360.

40 X. L. Su, J. R. Chen and G. P. Zheng, Three-dimensional porous activated carbon derived from loofah sponge biomass for supercapacitor applications, *Appl. Surf. Sci.*, 2018, **436**, 327.

41 X. L. Su, M. Y. Cheng and L. Fu, Superior supercapacitive performance of hollow activated carbon nanomesh with hier-archical structure derived from poplar catkins, *J. Power Sources*, 2017, **362**, 27.

42 X. L. Su, S. H. Li and S. Jiang, Superiorcapacitive behavior of porous activated carbon tubes derived from biomasswaste-cotonier strobili fibers, *Adv. Powder Technol.*, 2018, **29**, 2097.

43 A. Hai, G. Bharatha, K. Ram Babu, H. Taher, M. Naushad and F. Banat, Date seeds biomass-derived activated carbon for efficient removal of NaCl from saline solution, *Process Saf. Environ. Prot.*, 2019, **129**, 103.

44 N. L. Liu, S. Dutta and R. R. Salunkhe, ZIF-8 Derived, Nitrogen-doped porous electrodes of carbon polyhedron

particles for high-performance electrosorption of salt ions, *Sci. Rep.*, 2016, **6**, 1.

45 H. Li, T. Lu, L. Pan, Y. Zhang and Z. Sun, Electrosorption behavior of graphene in NaCl solutions, *J. Mater. Chem.*, 2009, **19**, 6773–6779.

46 C. Zhao, G. Liu, N. Sun, X. Zhang, G. Wang, Y. Zhang, H. Zhang and H. Zhao, Biomass-Derived N-Doped Porous Carbon as Electrode Materials for Zn-Air Battery Powered Capacitive Deionization, *Chem. Eng. J.*, 2018, **334**, 1270–1280.

